Energy Conversion and Management 169 (2018) 345–358

Contents lists available at ScienceDirect

Energy Conversion and Management

journal homepage: www.elsevier.com/locate/enconman

An improved explicit double-diode model of solar cells: Fitness verification and parameter extraction

Yujie Chen, Yize Sun*, Zhuo Meng

College of Mechanical Engineering, Donghua University, No. 2999 North Renmin Road, Songjiang, Shanghai 201620, China

ARTICLE INFO

Keywords:
Solar cells
Double-diode model
Explicit model
Parameter extraction
Teaching-learning-based optimization algorithm

ABSTRACT

Accurate simulation of photovoltaic characteristics is now a mandatory obligation before validating an experiment; hence, accurate model and parameters of solar cells are indispensable. This paper presents an improved explicit double-diode model based on the Lambert W function (EDDM-LW), and then compares the fitness and parameter extraction performance. By defining two new parameters (κ and τ) to separate the exponential function in double-diode model (DDM) and using the Lambert W function, the explicit expression for *I-V* characteristics is proposed. In contrast to exiting works, the new parameters can readily be computed by the electrical characteristics of the standard test condition without an implicit characteristic. To verify the accuracy of the proposed model, the fitness difference is first investigated with a solar cell and three different types of solar modules. The results indicate that under the same parameter values, EDDM-LW achieves the lowest root mean square error value and exhibits better fitness in representing the *I-V* characteristics. In addition, the optimal parameters are extracted by an improved teaching-learning-based optimization algorithm. The experimental results show that the optimal parameter values extracted from EDDM-LW are more accurate than those extracted from DDM. Based on these observations, EDDM-LW can be deemed a useful and practical model for the simulation, evaluation, and optimization of the photovoltaic system.

1. Introduction

Because of a decrease in conventional energy resources and an increase in environmental pollution, solar energy has increasingly received more international support and attention as a type of green energy. In addition, research has focused on improving the quality of solar cells and the efficiency of photovoltaic (PV) generation systems [1]. To predict the behavior of the PV system and optimally utilize the available solar energy, an efficient and accurate simulation model is indispensable [2]. With such a model, the characteristics of solar cells can be precisely emulated; that is, the calculated values fit the measured *I-V* data under all conditions, which is useful for production process improvement, simulation [3], evaluation and maximum energy harvesting of the PV system [4].

Over the years, many models have been published in the literature, and two equivalent circuit models are commonly used: single-diode model (SDM) [5] and double-diode model (DDM) [6]. DDM considers the composite effect of the neutral region and the space charge regions of the junction. Therefore, it can characterize the solar cells more accurately [7]. However, DDM is an implicit nonlinear transcendental equation and has seven unknown parameters. The inherent nature of this model hampers not only solar cell parameter extraction but also PV system simulation [8]. Therefore, many scholars have proposed various methods to extract the optimal parameters for the accurate simulation of PV characteristics, all of which can be divided into analytical methods [9] and metaheuristic algorithms [10].

Because of the complexity of DDM, the analytical methods usually solve the problem by reducing the number of parameters or assuming the parameter dimension. Ishaque et al. [11] assumed that the values of both saturation currents are equal ($I_{o1} = I_{o2}$), while one of the diode ideality factors was assigned as 1, thereby decreasing the number of parameters to five. However, equating the two currents does not make any physical sense. Babu et al. [12] and Hejri et al. [13] simplified the model by neglecting the parallel resistance or series resistance. However, these parameters greatly affect the model accuracy, especially in the vicinity of the open circuit voltage. The analytical method is simple and fast. However, the subjective hypothesis and omitted parameters affect the model's accuracy.

Metaheuristic algorithms impose no restrictions on the problem formulation; thus, numerous metaheuristic algorithms or their variants have been applied to the parameters identification of solar cells. Some of the optimization techniques are as follows: simulated annealing (SA)

* Corresponding author.
E-mail address: sunyz@dhu.edu.cn (Y. Sun).

https://doi.org/10.1016/j.enconman.2018.05.035
Received 13 February 2018; Received in revised form 16 April 2018; Accepted 10 May 2018
Available online 26 May 2018
0196-8904/

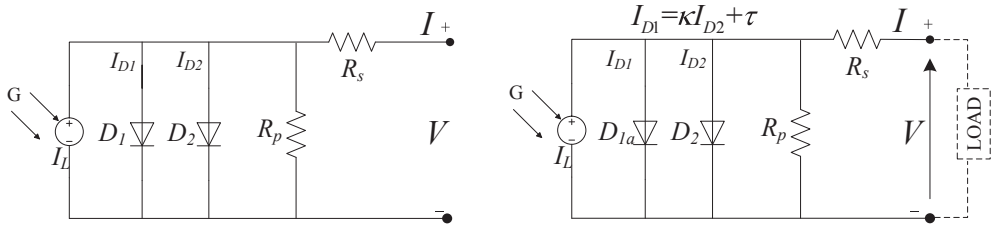

(a) Double-diode model [31] (b) The improved double-diode model

Fig. 1. Equivalent circuit of a solar cell under illumination.

[14], differential evolution (DE) [15], penalty-based differential evolution (P-DE) [16], artificial bee swarm optimization (ABSO) [17], flower pollination algorithm (FPA) [18], bird mating optimization (BMO) [19], partial swarm optimization (PSO) [20], artificial bee colony (ABC) [21], chaotic asexual reproduction optimization (CARO) [22], simplified swarm optimization (SSO) [23], and so on. However, DDM is an implicit nonlinear transcendental equation. In the calculation process, the measured current value is used as the original data to solve for the calculated current value. The implicit coupling relationship reduces the calculation accuracy.

Inspired by the superiority of the exact explicit single-diode model with more accurate *I-V* characteristics [24], maximum power point tracking (MPPT) [25], and efficient model parameter extraction [26], in recent years, the exact explicit expressions of DDM with two Lambert W function have been developed. Lugo-Munoz et al. [27] proposed a nonequivalent-R_s-connected two-diode model, which split the series resistance into two parts (R_{s1a}, R_{s1a}) and connected them to the diodes directly, thereby establishing an alternative model. Ortiz-Conde et al. [28] proposed another alternative model of DDM. The circuit was substituted by two equivalent resistances (a_1R_{TH}, a_2R_{TH}) in series with each of the two diodes. However, these alternative models are only approximations of DDM, because they are not exactly analogous for all possible arbitrary sets of parameters. Moreover, the extra parameters of these alternative models make parameter extraction even more difficult. Thus, some explicit expressions which maintain the original parameters and loyal to DDM have been developed.

Lun et al. [29] proposed a new explicit double-diode modeling method based on the assumption that both diode ideality factors were equal ($n_1 = n_2$). However, the relationship has no physical basis and is not always reliable. Dehghanzadeh et al. [30] proposed an approximate explicit double-diode model. A piecewise linear model was employed to approximate the two diodes. Unfortunately, the new parameter (a) cannot be generally defined by a mathematical function, which also results in parameter extraction difficulty. Gao et al. [31] proposed a Lambert W function based on the exact representation (LBER) for DDM. In this work, a vector r was defined as the Lambert W function coefficient, which was denoted by the ratio of the diffusion current to the sum of the diffusion and recombination currents. LBER is derived without an approximation and has a high precision. Regrettably, r is a change variable and is closely related to the terminal current and terminal voltage. Therefore, LBER still has an implicit characteristic. As compared to the alternative models, these new explicit solutions of DDM retain the concept and values of conventional double-diode parameters. However, the new parameter is either difficult to solve or has implicit features.

In light of the preceding discussions, this paper proposes an improved explicit double-diode model based on the Lambert W function (EDDM-LW) of solar cells. In contrast to existing works, the new parameters for the coefficients of the Lambert W function can readily be computed by the electrical characteristics of the standard test condition (STC), which leads to the fact that EDDM-LW contains only seven parameters identical to those included in DDM and does not exhibit an implicit characteristic. Moreover, it is derived from the general model DDM and should therefore suitable for various solar cells. To verify the accuracy of EDDM-LW, the proposed model is first investigated on the fitness difference among EDDM-LW, DDM and LBER under the same parameter values of the solar cells. It is implemented on the reported parameter values and experimental *I-V* data of a solar cell and three types of solar modules: commercial RTC France silicon solar cell [32], mono-crystalline (SM55) module [33], multi-crystalline (S75) module [34], and thin-film (ST40) module [35]. This paper then investigates the parameters exaction performance of EDDM-LW. An improved teaching-learning-based optimization (ITLBO) algorithm is employed for parameter extraction of EDDM-LW with the aim of validating the higher accuracy of the optimal parameter values extracted from EDDM-LW as compared those extracted from DDM.

The remainder of this paper is structured as follows. Section 2 describes the derivation of the EDDM-LW in detail. Section 3 investigates the fitness difference of the EDDM-LW with DDM and LBER. Section 4 presents an ITLBO algorithm base on the hybrid strategy. This is followed by the parameter extraction results, simulated curves and discussions in Section 5. Finally, Section 6 presents the conclusions.

2. Explicit double-diode model based on the Lambert W function (EDDM-LW)

2.1. Double-diode model

DDM [36] is one of the most popular models because of its accurate representation of solar cell characteristics, especially at low illumination levels. It is widely used for first- and second-generation PVs [37]. The equivalent circuit of DDM represented in Fig. 1(a). The two diodes reflect the physical phenomena of the P-N junction. One indicates the diffusion process whereas the other shows the composite effect of the space charge regions. Series resistance represents initial losses and shunt resistance represents the modeling of the reverse saturation current [30].

According to Kirchhoff's current law, the *I-V* relationship can be represented by the following DDM Eq. (1).

$$I = I_L - I_{D1} - I_{D2} - \frac{V + IR_s}{R_p} \tag{1}$$

where I is the terminal current; V is the terminal voltage; I_L is the photo-generated current; I_{D1} and I_{D2} define the diffusion and recombination currents, respectively; R_s is the series resistance; and R_p is the shunt resistance. In addition, according to the Shockley equation, I_{D1} and I_{D2} can be expressed as follows:

$$I_{D1} = I_{o1}\left[\exp\left(\frac{V + IR_s}{n_1 V_{th}}\right) - 1\right] \tag{2}$$

$$I_{D2} = I_{o2}\left[\exp\left(\frac{V + IR_s}{n_2 V_{th}}\right) - 1\right] \tag{3}$$

where n_1 and n_2 are the diode ideality factors; I_{o1} and I_{o2} are the

Table 1
RMSE values of DDM, LBER and EDDM-LW using the published parameter values of various algorithms for the RTC France solar cell.

	GOFPANM [40]	R_{cr}-IJADE [41]	CSO [42]	BMO [43]	SATLBO [44]	GOTLBO [45]	ABSO [17]	IGHS [46]	MSSO [23]	WDO [47]	FPA [18]
I_L(A)	0.7607811	0.760781	0.76078	0.76078	0.76078	0.760752	0.76078	0.76079	0.760748	0.7606	0.760795
I_{o1}(μA)	0.7493476	0.225974	0.22732	0.2111	0.25093	0.800195	0.26713	0.97310	0.234925	0.2531	0.300088
I_{o2}(μA)	0.2259743	0.749347	0.72785	0.87688	0.545418	0.220462	0.38191	0.16791	0.671593	0.0482	0.166159
R_s(Ω)	0.0367404	0.03674	0.036737	0.03682	0.03663	0.036783	0.03657	0.03690	0.036688	0.037433	0.0363342
R_p(Ω)	55.485449	55.485443	55.3813	55.8081	55.117	56.0753	54.6219	56.8368	55.714662	52.6608	52.3475
n_1	2	1.451017	1.45151	1.44533	1.45982	1.999973	1.46512	1.92126	1.454255	1.51162	1.47477
n_2	1.4510168	2	1.99769	1.99997	1.99941	1.448974	1.98152	1.42814	1.995305	1.38434	2
$RMSE_{DDM}$ (E-03)	0.982485	0.982486	0.982532	0.982661	0.982941	0.983152	0.983599	0.986572	1.059101	1.095213	1.24239
$RMSE_{LBER}$ (E-03)	0.757771	0.757776	0.757941	0.754967	0.762587	0.757262	0.765586	0.756810	0.795115	0.83879	0.88949
$RMSE_{EDDM-LW}$ (E-03)	0.753770	0.754058	0.754387	0.751599	0.759226	0.754412	0.762913	0.751928	0.784885	0.83819	0.88468

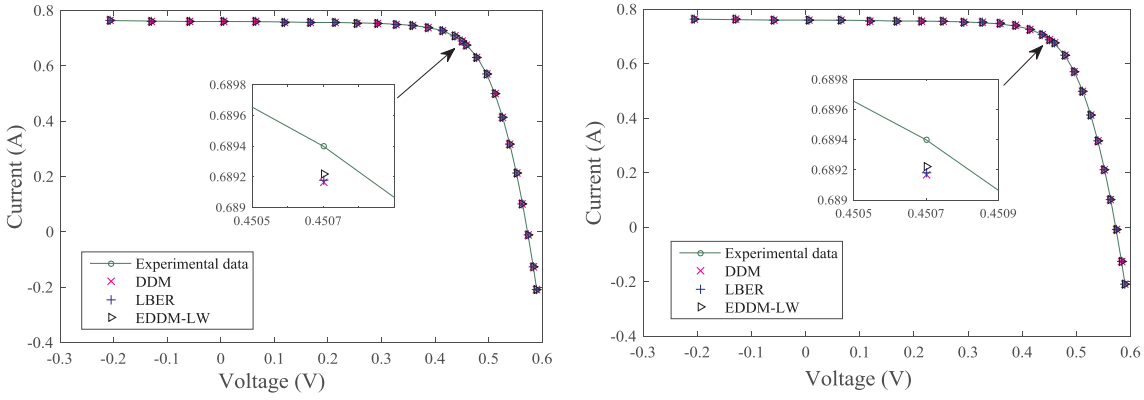

Fig. 2. Comparison of the calculated curves based on DDM, LBER, and EDDM-LW models for the RTC France solar cell by two different algorithms.

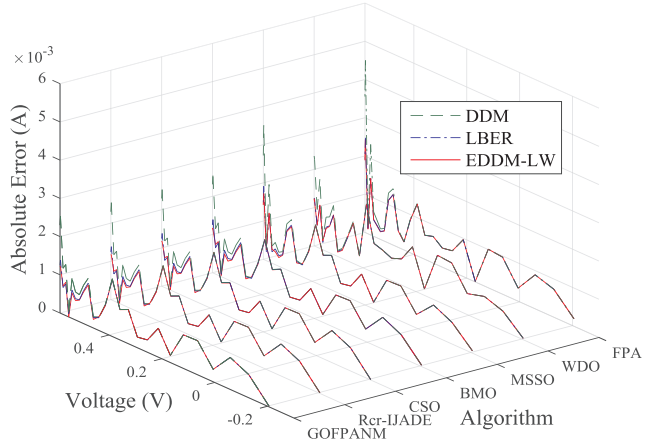

Fig. 3. Comparison of the absolute current errors based on DDM, LBER, and EDDM-LW models for the RTC France solar cell by several algorithms.

saturation currents of the equivalent diodes; V_{th} is the thermal voltage, which is given by $V_{th} = kT/q$. Here k is the Boltzmann constant, 1.3806503E-23, T is the working absolute temperature of the cells, and q is the electron charge, 1.60217646E-19.

As presented in Eqs. (1)–(3), DDM is an implicit nonlinear transcendental equation that has seven unknown parameters. In addition, the model has two exponential functions. Solving the model based solely on elementary functions and the Lambert W function is difficult. Therefore, it is first necessary to decouple the two exponential terms of DDM, then an explicit model of a solar cell can be generated by the Lambert W function.

Table 2
Solar modules specifications.

	Unit	Mono-crystalline (SM55)	Multi-crystalline (S75)	Thin-film (ST40)
$I_{SC,STC}$	A	3.45	4.7	2.68
$V_{OC,STC}$	V	21.7	21.6	22.9
$I_{MPP,STC}$	A	3.15	4.26	2.28
$V_{MPP,STC}$	V	17.4	17.6	15.8
K_I	mA/°C	1.40	2.00	0.32
K_V	mV/°C	−76.0	−76.0	−100
K_{IP}	mA/°C	0.14	0.14	0.45
K_{VP}	mV/°C	−76.0	−76.0	−100
N_s	–	36	36	42

2.2. Derivation of the proposed EDDM-LW

The two exponential terms significantly challenge the generation of an explicit double-diode model. According to Eqs. (2) and (3), the exponential terms can be expressed as follows:

$$\left(\frac{I_{D1}+I_{o1}}{I_{o1}}\right)^{n_1} = \exp\left(\frac{V+IR_s}{V_{th}}\right) \tag{4}$$

$$\left(\frac{I_{D2}+I_{o2}}{I_{o2}}\right)^{n_2} = \exp\left(\frac{V+IR_s}{V_{th}}\right) \tag{5}$$

The following relationship is then observed based on Eqs. (4) and (5):

$$\left(\frac{I_{D1}+I_{o1}}{I_{o1}}\right)^{n_1} = \left(\frac{I_{D2}+I_{o2}}{I_{o2}}\right)^{n_2} \tag{6}$$

Simplifying Eq. (6), the current relationship between two diodes can then be obtained:

Table 3
RMSE values of DDM, LBER, and EDDM-LW using the published parameter values extracted by R_{cr}-IJADE [31] and FPA [18] for solar module SM55.

Irrad. & Temp.	Algorithms	I_L(A)	I_{o1}(A)	I_{o2}(A)	R_s(Ω)	R_p(Ω)	n_1	n_2	$RMSE_{DDM}$	$RMSE_{LBER}$	$RMSE_{EDDM-LW}$
200 W/m^2, 25 °C	R_{cr}-IJADE	0.6944	1.2537E-09	4.8517E-09	0.5445	366.6775	1.1391	1.1574	0.003601	0.0031591	0.0031591
	FPA	0.69058	1.3987E-07	1.41907E-07	0.3390	443.4634	1.378175	3.45683	0.020650	0.0186500	0.0186498
400 W/m^2, 25 °C	R_{cr}-IJADE	1.3882	3.4151E-10	5.0629E-10	0.7258	345.7318	1.0061	1.4986	0.008657	0.0060954	0.0060938
	FPA	1.380696	1.3922E-07	1.21521E-07	0.338684	451.183	1.377924	2.29726	0.016838	0.0150283	0.0150270
600 W/m^2, 25 °C	R_{cr}-IJADE	2.0799	2.6544E-10	2.758E-10	0.6344	361.8583	1.0002	1.2180	0.009622	0.0075880	0.0075792
	FPA	2.068947	1.4724E-07	1.53021E-07	0.338031	480.1678	1.38245	2.834106	0.019395	0.0166963	0.0166951
800 W/m^2, 25 °C	R_{cr}-IJADE	2.7687	4.7332E-10	2.5047E-10	0.5412	398.9244	1.0280	1.2359	0.012462	0.0095439	0.0095391
	FPA	2.759354	1.4255E-07	6.75512E-07	0.338823	469.336	1.37918	3.14591	0.036456	0.0263848	0.0263801
1000 W/m^2, 25 °C	R_{cr}-IJADE	3.4589	3.3008E-10	1.2343E-09	0.5073	334.0537	1.0152	1.3790	0.020555	0.0139124	0.0139029
	FPA	3.450253	1.3024E-07	3.59717E-07	0.339257	442.917	1.37302	2.11451	0.058579	0.0387231	0.0386919
1000 W/m^2, 40 °C	R_{cr}-IJADE	3.4709	8.5126E-09	1.7289E-07	0.4984	330.0379	1.0762	1.5082	0.015625	0.0112120	0.0112101
	FPA	3.46798	7.2581 E-07	6.68113E-07	0.338999	454.9449	1.37801	3.896155	0.042017	0.0243517	0.0243507
1000 W/m^2, 60 °C	R_{cr}-IJADE	3.4780	7.2722E-08	1.0075E-06	0.4879	400.3159	1.0633	1.3600	0.012940	0.0106876	0.0106875
	FPA	3.49099	5.2417E-06	2.0854E-05	0.33898	470.6224	1.378047	3.56047	0.024479	0.0164308	0.0164134

Table 4
RMSE values of DDM, LBER, and EDDM-LW using the published parameter values extracted by GOFPANM [40] for solar module S75.

Irrad. & Temp.	I_L(A)	I_{o1}(μA)	I_{o2}(μA)	R_s(Ω)	R_p(Ω)	n_1	n_2	$RMSE_{DDM}$	$RMSE_{LBER}$	$RMSE_{EDDM-LW}$
200 W/m^2,25 °C	0.944112	0.130362	2.51873E-02	0.263522	411.6936	2.708126	1.234112	0.003625	0.0035528	0.0035528
400 W/m^2,25 °C	1.884222	0.604725	6.35887E-03	0.264344	350.0834	4.000000	1.140587	0.011655	0.0086655	0.0086646
600 W/m^2,25 °C	2.829828	7 .229E-05	6.0509E-04	0.393193	298.0491	1.00028	1.034755	0.0234797	0.0140233	0.0140206
800 W/m^2,25 °C	3.75642	0.615608	3.27397E-03	0.35178	425.9434	3.93972	1.106675	0.0230519	0.0157443	0.0157437
1000 W/m^2,25 °C	4.6967	0.101298	2.42065E-02	0.25968	373.6218	3.568125	1.22198	0.025270	0.0166301	0.0166299
1000 W/m^2,50 °C	4.732801	1.00000	1.00000	0.269543	2553.9525	1.345303	1.3453.74	0.0350965	0.0231249	0.0231248
1000 W/m^2,60 °C	4.755886	1.00000	1.00000	0.3150663	931.74878	1.258305	1.258315	0.0460539	0.0278476	0.0278476

Table 5
RMSE values of DDM, LBER, and EDDM-LW using the published parameter values extracted by GOFPANM [40] and FPA [18] for solar module ST40.

Irrad. & Temp.	Algorithms	I_L(A)	I_{o1}(A)	I_{o2}(A)	R_s(Ω)	R_p(Ω)	n_1	n_2	$RMSE_{DDM}$	$RMSE_{LBER}$	$RMSE_{EDDM-LW}$
200 W/m^2, 25 °C	GOFPANM	0.54465	1.00000	1.00000	1.82482	377.09409	1.51665	1.51665	0.0074046	0.0066069	0.0066069
	FPA	0.53285	1.28671	1.503562	1.140772	314.2327	1.484785	3.101258	0.0215056	0.0200063	0.0200059
400 W/m^2, 25 °C	GOFPANM	1.08112	0.99965	0.99943	1.21380	346.5713	1.52591	1.52915	0.0081502	0.00723406	0.00723406
	FPA	1.07111	0.8122822	74.71976	1.147978	322.0261	1.438419	3.678599	0.0216147	0.0179175	0.0178758
600 W/m^2, 25 °C	GOFPANM	1.6190	1.00000	0.99999	1.13603	303.5947	1.52940	1.52938	0.0127779	0.0104779	0.0104779
	FPA	1.60615	1.1969	47.38319	1.123132	339.4545	1.47787	3.60533	0.0190654	0.0163257	0.0163249
800 W/m^2, 25 °C	GOFPANM	2.16336	0.99999	0.99999	1.04734	220.6717	1.53167	1.53174	0.0146988	0.0115680	0.0115679
	FPA	2.14352	1.035084	1.125682	1.138831	313.8327	1.462271	3.305267	0.0197221	0.0157863	0.0157863
1000 W/m^2, 25 °C	GOFPANM	2.70363	0.13907	1.1574E-03	1.31879	217.1629	1.33602	1.04968	0.0192127	0.0121669	0.0121665
	FPA	2.67805	1.19606	62.2786	1.121674	332.9976	1.477328	3.724013	0.0574231	0.0292468	0.0291811
1000 W/m^2, 40 °C	GOFPANM	2.7374	0.99999	0.99999	1.15412	168.2621	1.36711	1.36689	0.0176972	0.0127064	0.0127064
	FPA	2.68299	4.657815	36.76408	1.135602	332.0241	1.457196	2.80591	0.0330757	0.0295551	0.0295528

$$I_{D1} + I_{o1} = \frac{I_{o1}}{I_{o2}^{n_2/n_1}}(I_{D2} + I_{o2})^{n_2/n_1} \tag{7}$$

Because the values of I_{o1} and I_{o2} are quite small, their influence on I_{D1} and I_{D2} can be neglected. Setting $a = I_{o1}/I_{o2}^{n_2/n_1}$ and $b = n_2/n_1$. Eq. (7) can be rewritten as follows to define the relationship between I_{D1} and I_{D2}:

$$I_{D1} = aI_{D2}^{b} \tag{8}$$

Based on Eq. (8), the exponential terms in DDM can be separated. For convenience of calculation, Eq. (8) can be simplified into a polynomial of degree 1 as follows:

$$I_{D1} = \kappa I_{D2} + \tau \tag{9}$$

According to the electrical characteristics of the STC, short-circuit current, open-circuit voltage, maximum power point (MPP) current, and MPP voltage at different irradiances and temperatures can be calculated using Eqs. (10)–(13) [38], respectively. Three different sets of diode currents (I_{D1_SC}, I_{D2_SC}), (I_{D1_OC}, I_{D2_OC}), and (I_{D1_mpp}, I_{D2_mpp}) can then be obtained. The least square method can be employed to fit the three data sets to solve coefficients κ and τ.

$$I_{SC} = I_{SC,STC}\frac{G}{G_{STC}}[1 + K_I(T - T_{STC})] \tag{10}$$

$$V_{OC} = V_{OC,STC} + V_{th}\ln\frac{G}{G_{STC}} + K_V(T - T_{STC}) \tag{11}$$

$$I_{mpp} = I_{mpp,STC}\frac{G}{G_{STC}}[1 + K_{IP}(T - T_{STC})] \tag{12}$$

$$V_{mpp} = V_{\mathrm{mpp},STC} + V_{th}\ln\frac{G}{G_{STC}} + K_{VP}(T - T_{STC}) \tag{13}$$

where I_{SC_STC}, V_{OC_STC}, I_{mpp_STC}, V_{mpp_STC}, G_{STC}, and T_{STC} are the short-circuit current, open-circuit voltage, MPP current, MPP voltage, irradiance, and temperature at the STC, respectively; G is the solar irradiance, T is the temperature; and K_I, K_V, K_{IP}, and K_{VP} are the temperature coefficients of short-circuit current, open-circuit voltage, MPP current, and MPP voltage, respectively.

Substituting Eq. (9) into the equivalent model of the double-diode, Eq. (1) can then be split into two formulas, Eqs. (14) and (15):

$$I = I_L - \frac{\kappa + 1}{\kappa}\cdot I_{o1}\left[\exp\left(\frac{V + IR_s}{n_1 V_{th}}\right) - 1\right] + \frac{\tau}{\kappa} - \frac{V + IR_s}{R_p} \tag{14}$$

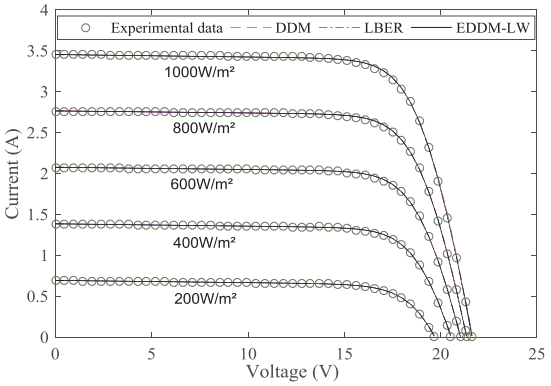

(a) *I-V* characteristics at different irradiances

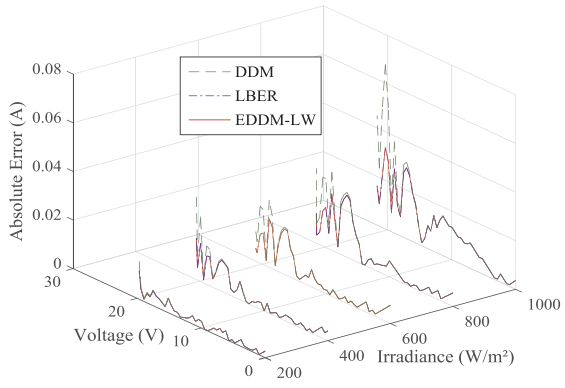

(b) Absolute current errors at different irradiances

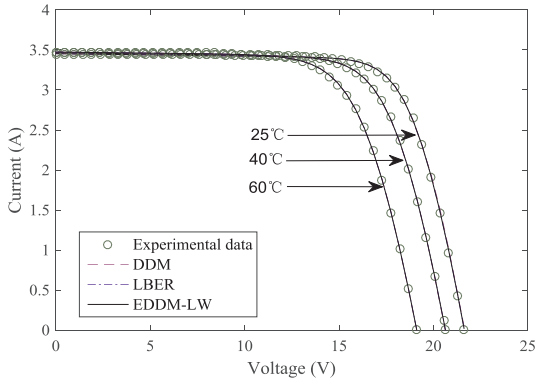

(c) *I-V* characteristics at different temperatures

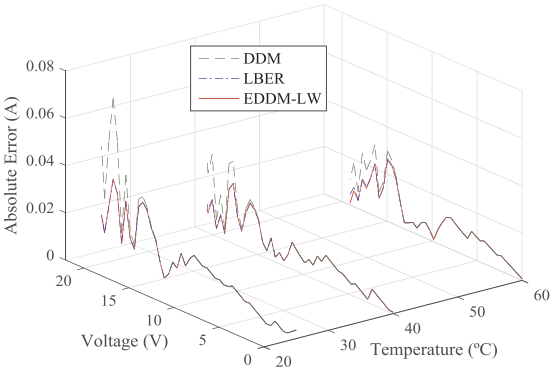

(d) Absolute current errors at different temperatures

Fig. 4. Calculated curves based on DDM, LBER, and EDDM-LW using the parameter values extracted by R_{cr}-IJADE for solar module SM55.

$$I = I_L - (\kappa + 1)\cdot I_{o2}\left[\exp\left(\frac{V + IR_s}{n_2 V_{th}}\right) - 1\right] - \tau - \frac{V + IR_s}{R_p} \tag{15}$$

Eqs. (14) and (15) can then be treated as the decomposition equations of DDM. Both equations have only one exponential term. Therefore, the terminal current can be expediently expressed by the Lambert W function [39].

$$I = \frac{R_p(I_L + \frac{\tau}{\kappa} + \frac{\kappa+1}{\kappa}\cdot I_{o1}) - V}{R_s + R_p} - \frac{n_1 V_{th}}{R_s} W(x_1) \tag{16}$$

$$I = \frac{R_p[I_L - \tau + (\kappa + 1)\cdot I_{o2}] - V}{R_s + R_p} - \frac{n_2 V_{th}}{R_s} W(x_2) \tag{17}$$

where

$$x_1 = \frac{\frac{\kappa+1}{\kappa}\cdot I_{o1} R_s R_p}{n_1 V_{th}(R_s + R_p)} \exp\left\{\frac{R_p\left[R_s(I_L + \frac{\tau}{\kappa}) + \frac{\kappa+1}{\kappa}\cdot I_{o1} R_s + V\right]}{n_1 V_{th}(R_s + R_p)}\right\} \tag{18}$$

$$x_2 = \frac{(\kappa + 1) I_{o2} R_s R_p}{n_2 V_{th}(R_s + R_p)} \exp\left\{\frac{R_p[R_s(I_L - \tau) + (\kappa + 1)\cdot I_{o2} R_s + V]}{n_2 V_{th}(R_s + R_p)}\right\} \tag{19}$$

Dividing the both side of Eq. (16) by $\frac{\kappa+1}{\kappa}$, Eq. (17) by $\kappa + 1$, and adding them term by term, the explicit double-diode model based on the Lambert W function (EDDM-LW) can be observed.

$$I = \frac{R_p(I_L + I_{o1} + I_{o2}) - V}{R_s + R_p} - \frac{V_{th}}{R_s}\left[\frac{\kappa}{\kappa + 1} n_1 W(x_1) + \frac{1}{\kappa + 1} n_2 W(x_2)\right] \tag{20}$$

3. Fitness verification of the EDDM-LW

The proposed EDDM-LW eliminates the implicit coupling relations between the current and the voltage, and establishes the explicit analytic expression of the current and the voltage. However, the model still exhibits some errors because of the difference between the Lambert W and the exponential function, and the approximate relationship between the diffusion current and recombination current. To verify the accuracy of EDDM-LW, the fitness difference is carried out among EDDM-LW, DDM and LBER [31]. It is designed to investigate which model can best represent the *I-V* characteristic under the same parameter values. Specifically, LBER is the only explicit model that contains seven parameters identical to those included in DDM. The superiority of LBER has been demonstrated in Ref. [31]. Therefore, this paper covers only the fitness comparison among EDDM-LW, DDM and LBER, which are denoted in the following subsections.

3.1. Verification function

The main objective of model establishment and parameter extraction is the minimization of the current errors between calculated and experimental values. The individual absolute errors (IAE) between the calculated current and experimental current of EDDM-LW, DDM and LBER can be respectively expressed as follows:

$$IAE_{EDDM-LW} = \left| \frac{R_p(I_L + I_{o1} + I_{o2}) - V}{R_s + R_p} - \frac{V_{th}}{R_s}\left[\frac{\kappa}{\kappa + 1} n_1 W(x_1) + \frac{1}{\kappa + 1} n_2 W(x_2)\right] - I \right| \tag{21}$$

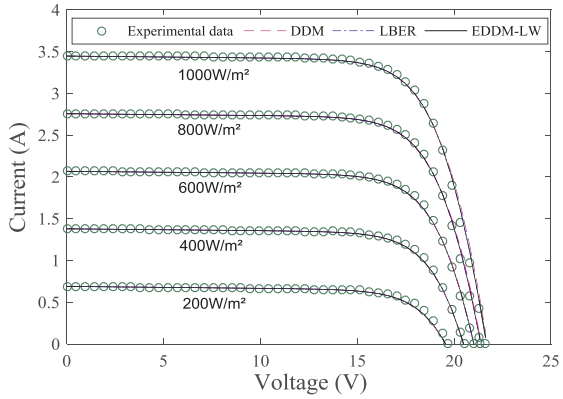

(a) *I-V* characteristics at different irradiances

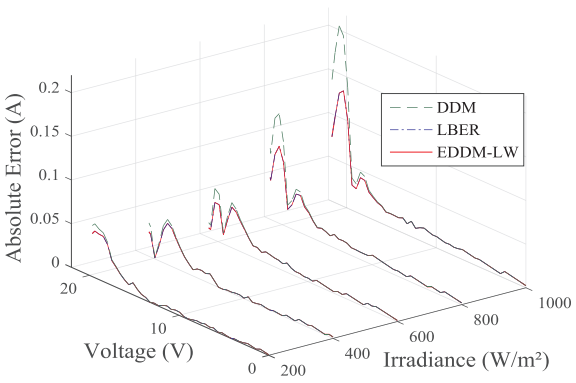

(b) Absolute current errors at different irradiances

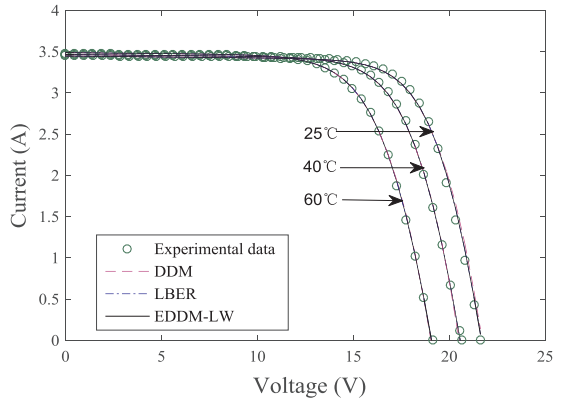

(c) *I-V* characteristics at different temperatures

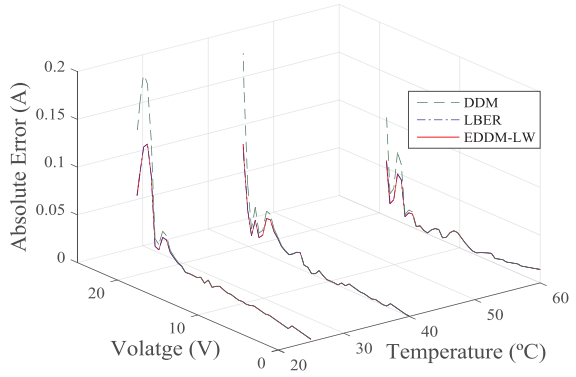

(d) Absolute current errors at different temperatures

Fig. 5. Calculated curves based on DDM, LBER and EDDM-LW using the parameter values extracted by FDA for solar module SM55.

$$IAE_{DDM} = \left| I_L - I_{o1}\left[\exp\left(\frac{V+IR_s}{n_1V_{th}}\right)-1\right] - I_{o2}\left[\exp\left(\frac{V+IR_s}{n_2V_{th}}\right)-1\right] - \frac{V+IR_s}{R_p} - I \right| \tag{22}$$

$$IAE_{LBER} = \left| \frac{R_p(I_L+I_{o1}+I_{o2})-V}{R_s+R_p} - r\frac{n_1V_{th}}{R_s}W(\theta_1) - (1-r)\frac{n_2V_{th}}{R_s}W(\theta_2) - I \right| \tag{23}$$

where

$$\theta_1 = \frac{I_{o1}R_sR_p}{rn_1V_{th}(R_s+R_p)}\exp\left[\frac{R_p(R_sI_L+I_{o1}R_s/r+V)}{n_1V_{th}(R_s+R_p)}\right] \tag{24}$$

$$\theta_2 = \frac{I_{o2}R_sR_p}{(1-r)n_2V_{th}(R_s+R_p)}\exp\left[\frac{R_p(R_sI_L+I_{o2}R_s/(1-r)+V)}{n_2V_{th}(R_s+R_p)}\right] \tag{25}$$

$$r = \frac{I_{o1}\left[\exp\left(\frac{V+IR_s}{n_1V_{th}}\right)-1\right]}{I_{o1}\left[\exp\left(\frac{V+IR_s}{n_1V_{th}}\right)-1\right] + I_{o2}\left[\exp\left(\frac{V+IR_s}{n_2V_{th}}\right)-1\right]} \tag{26}$$

Similar to Refs. [38–47], the root mean square error (RMSE) is used as the fundamental measure of curve fit accuracy. Obviously, under the same parameter values, smaller RMSE value corresponds to better experimental *I-V* data fitness. Hence, the verification function is formulated as follows:

$$RMSE = \sqrt{\frac{1}{N}\sum_{i=1}^{N}(I_{calculate}-I)^2} \tag{27}$$

where N is the number of experimental data; $I_{calculate}$ is the calculated current obtained through the model; I is the experimental current.

3.2. Fitness comparison results for the solar cell

The solar cell presents for fitness comparison is a 57-mm diameter commercial RTC France silicon solar cell, which is described in Ref. [32]. The experimental *I-V* data is detected under an irradiance of 1000 W/m^2 and a temperature of 33 ˚C. The characteristic points at the experimental condition are as follows: open-circuit voltage (0.5728 V), short-circuit current (0.7603 A), MPP voltage (0.4507 V), and MPP current (0.6894 A). Based on these data, many scholars use a variety of algorithms to extract the parameter of DDM. Table 1 enumerates 11 parameter values that are originally published in the references and named with their respective algorithms.

The RMSE values of EDDM-LW, DDM and LBER are calculated by Eqs. (21)–(27), and are summarized in the last three rows of Table 1. As can be seen in the table, the RMSE values based on EDDM-LW are obviously lower than the RMSE values of DDM and are slightly lower than the RMSE values of LBER. On this basis, we select the better two groups of parameter values and draw the comparison between the calculated curves and experimental data, as shown in Fig. 2. In the partially enlarged view, the calculative current based on the proposed model EDDM-LW is closer to the experimental current at the maximum power point. The conclusion can be drawn that the proposed EDDM-LW would be beneficial for the MPPT of the PV system.

In addition, Fig. 3 presents a plot of the absolute current errors for the different parameter values extracted by various algorithms. It is clear that the absolute current errors of the explicit model (EDDM-LW, LBER) are smaller than the errors of the implicit model DDM. In particular, when the terminal voltages exceed 0.4 V, the increase in the absolute current errors of DDM is obvious, and the absolute current

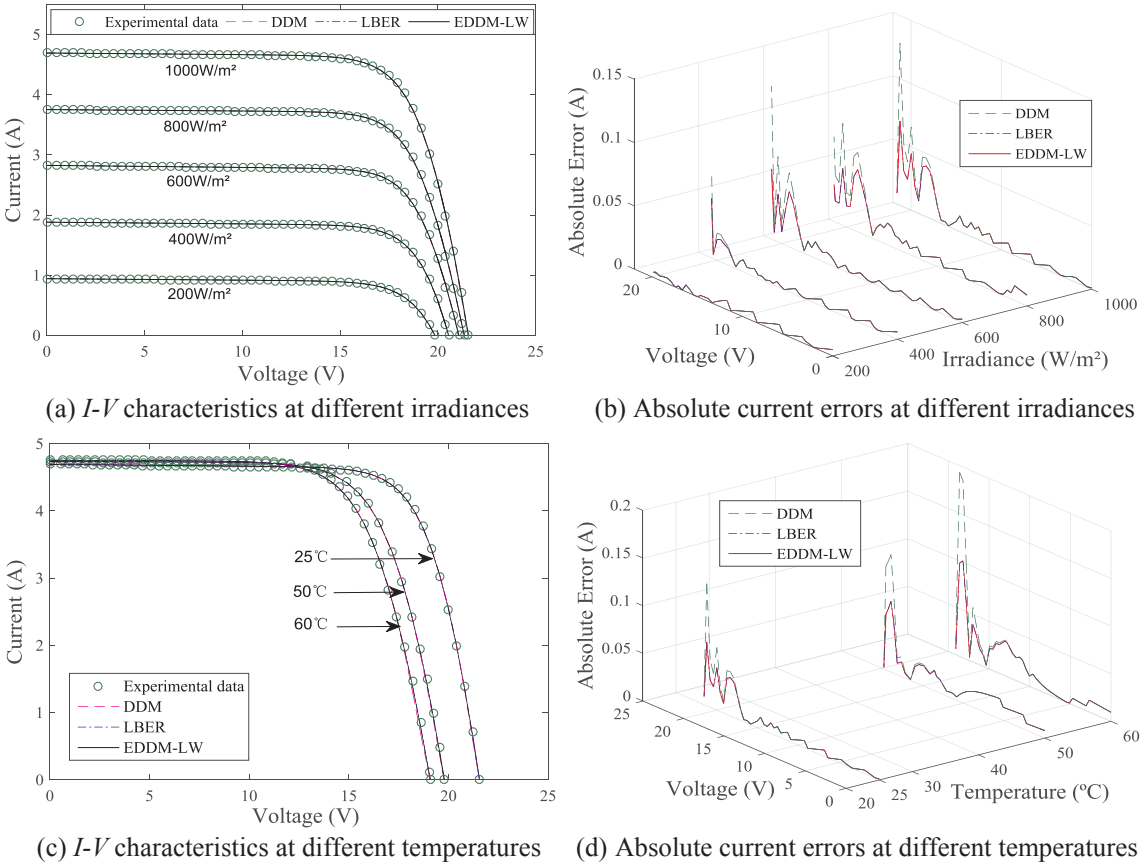

(a) *I-V* characteristics at different irradiances

(b) Absolute current errors at different irradiances

(c) *I-V* characteristics at different temperatures

(d) Absolute current errors at different temperatures

Fig. 6. Calculated curves based on DDM, LBER, and EDDM-LW using the parameter values extracted by GOFPANM for solar module S75.

errors of EDDM-LW are slightly lower than those of LBER, thereby indicating that the proposed model EDDM-LW exhibits the best fitted the experimental data under the same parameter values.

3.3. Fitness comparison results for the three different types of solar modules

Three different types of solar modules are used to verify the fitness of the three models, specifically the mono-crystalline (SM55) module [33], multi-crystalline (S75) module [34], and thin-film(ST40) module [35]. The experimental data of these solar modules are directly extracted from the manufacturer information sheets at five different irradiance levels (1000 W/m^2, 800 W/m^2, 600 W/m^2, 400 W/m^2, and 200 W/m^2), and different temperature levels. The specifications of these modules are summarized in Table 2.

Table 3 lists the reported parameter values extracted by R_{cr}-IJADE [26] and FPA [16] for solar module SM55. Table 4 lists the reported parameter values extracted by GOFPANM [34] for solar module S75. Table 5 lists the reported parameter values extracted by GOFPANM [34] and FPA [16] for solar module ST40. In addition, the last three columns of Tables 3–5 summarize the RMSE values of EDDM-LW, DDM, and LBER, which are calculated using Eqs. (21)–(27).

It can be observed that all the RMSE values of EDDM-LW are smaller than those of DDM and are slightly less than or equal to those of LBER. In addition to a decrease in the RMSE values, the difference between the models become smaller and smaller. Although the RMSE value of LBER is close to that of EDDM-LW, LBER still exhibits the implicit characteristic, which is eliminated in EDDM-LW. Moreover, any reduction in the RMSE value is significant, because it aids in the calculation of the real values of the parameters.

To further envisage the accuracy of EDDM-LW, the comparison of the *I-V* characteristics and the individual absolute current errors with EDDM-LW, DDM and LBER are carried out at varying irradiance and temperature levels. Figs. 4–8 are the calculated curves using the parameter values extracted by different algorithms for the three types of solar modules, respectively. From Figs. 4–8(a) and (c), it is obvious that for each irradiance and temperature value, the explicit models EDDM-LW and LBER are closer to the experimental data than DDM. In addition, a slight difference between EDDM-LW and LBER is observed. Similar results can be observed in Figs. 4–8(b) and (d).

Furthermore, according to Figs. 4–8(b) and (d), the absolute current errors in each model tend to increase following an increase of the terminal voltage, especially in the high-voltage range. In the low-voltage range, the absolute current errors are small and are almost the same for EDDM-LW, DDM and LBER. However, in the high-voltage range, the absolute current errors of EDDM-LW exhibit a significant gap as compared to DDM and are distinct from LBER, thereby indicating that the advantage of EDDM-LW is mainly reflected in the high-voltage region. In addition, from the comparison of the calculation curves of one solar module at different parameter values, more accurate the parameter values generate smaller differences among EDDM-LW, DDM and LBER.

In summary, these results demonstrate that the proposed EDDM-LW is correct and exhibits better fitness in representing the *I-V* characteristics of the solar cells. It is suitable for many different solar modules with varying irradiance and temperature levels. Therefore, as an improved model based on DDM, the proposed EDDM-LW can be beneficial for the simulation, analysis and optimization control of the PV system.

4. Improved teaching-learning-based optimization algorithm

To further investigate the performance of EDDM-LW, this section discusses the use of an improved teaching-learning-based optimization algorithm to extract the parameters of the proposed model. This paper assigned the RMSE as the optimizing objective, wherein Eq. (27) is

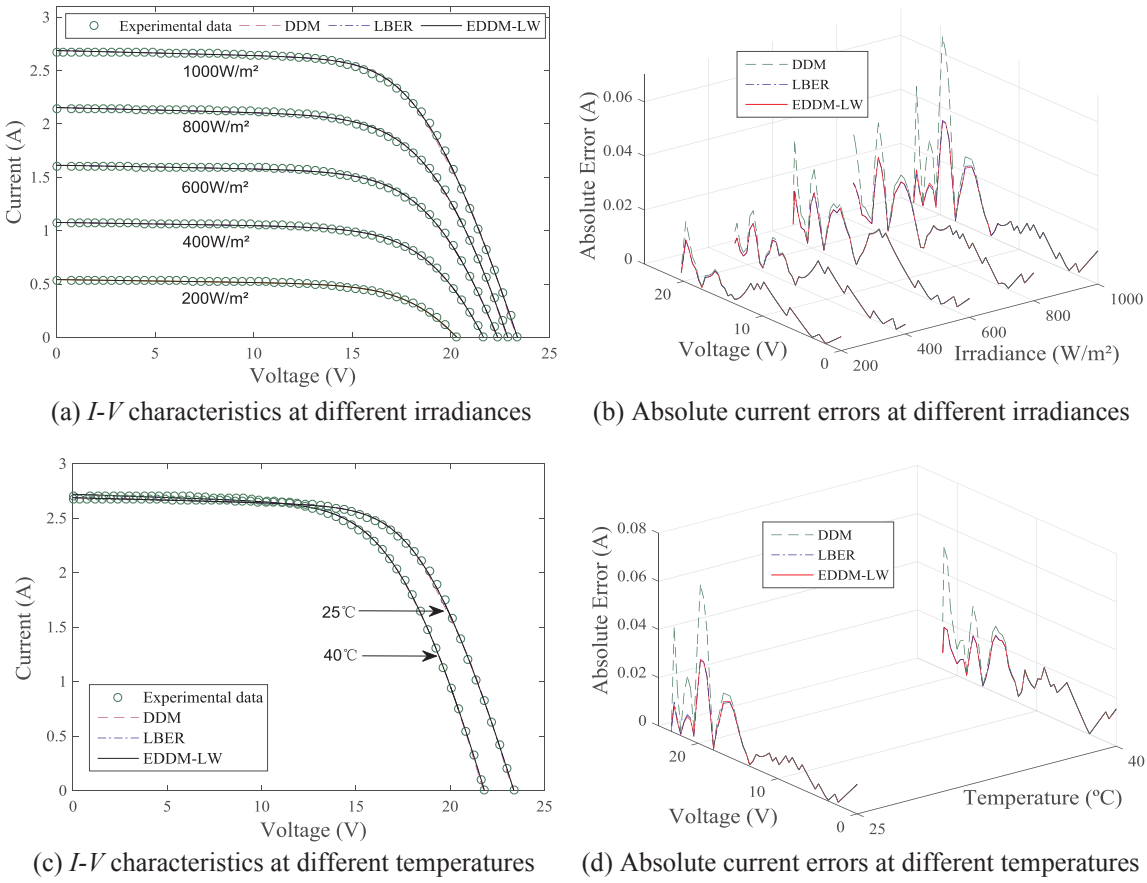

(a) *I-V* characteristics at different irradiances (b) Absolute current errors at different irradiances

(c) *I-V* characteristics at different temperatures (d) Absolute current errors at different temperatures

Fig. 7. Calculated curves based on DDM, LBER, and EDDM-LW using the parameter values extracted by GOFPANM for solar module ST40.

employed as the constraint equation to find the optimal parameters.

Teaching-learning-based optimization is a heuristic algorithm based on the population hunting strategy, which is proposed by Rao et al. [48]. This technique is characterized by a few detected parameters, a simple structure, and good exploration capability [49,50]. The algorithm is inspired by the classical teaching and learning process. In class, the teacher shares his or her knowledge to improve the performance of the whole class. Students can also learn from each other to improve their performance. The optimum solution of the objective function is derived by the simulation of this in-class process. The algorithm has three steps: the population initialization, the teacher phase, and the learner phase.

4.1. Population initialization

First, the student number and the boundary of performance are confirmed by initializing the grades of each student. This involves confirming the number of population particles *NP* and their initial values. To ensure the diversity of the individual in the decision-making space, the initial values of each particle are generated randomly as follows:

$$x_i^j = x_i^L + rand(0,1) \times (x_i^U - x_i^L)(j = 1,2,\cdots NP) \tag{28}$$

where $x^j = \{I_L^j, I_{o1}^j, I_{o2}^j, R_s^j, R_p^j, n_1^j, n_2^j\}(j = 1,2,\cdots NP)$

4.2. Teacher phase

In this phase, the teacher provides knowledge to the student. Students improve their performance using the difference between the teacher and the mean result of the class according each student's own capability. Teacher $x_{teacher}$ is the individual that gets the minimum RMSE value from Eq. (27), and the other individual are students. The teacher phase can be formulated as follows,

$$x_{new}^i = x_{old}^i + rand(0,1) \times (x_{teacher} - T_{Fi} \times mean) \tag{29}$$

where x_{old}^i and x_{new}^i are the students' old and new individual performance, *mean* is the mean of the current population, *rand*(0,1) is the step size of learning, and T_{Fi} is the teaching factor, which is given by $T_{Fi} = round[1 + rand(0,1)]$.

According to Eq. (29), it can be seen that T_{Fi} is the main factor in this stage. A large T_{Fi} improves the speed of the algorithm, but decreases the search ability. Conversely, a small T_{Fi} generates a more precise search but decreases speed [51]. Therefore, an adaptive teaching factor is introduced, which is dynamically adjusted to the average fitness value and decreased with iteration. The adaptive T_{Fi} can be formulated as follows:

$$T_{Fi} = T_{F\max} - \frac{(T_{F\max} - T_{F\min}) \cdot f_{avg}}{f} \cdot \frac{iter}{iter_{\max}} \tag{30}$$

where f is the *RSME* value of the ith particle, f_{avg} is the average *RSME* value of all particles, *iter* is the present number of iterations, and $iter_{\max}$ is the maximum number of iterations.

The new individual x_{new}^i will be accepted based on Eqs. (29) and (30) if it gives a smaller RMSE than the old individual.

4.3. Learner phase

In the learner phase, the student enhances his or her knowledge by randomly interacting with a different student. This is similar to the difference mutation operator, although the learning process of each student is different. Learner x^i randomly selects another learner x^j to study and the learner phase can be expressed by Eq. (31) as follows:

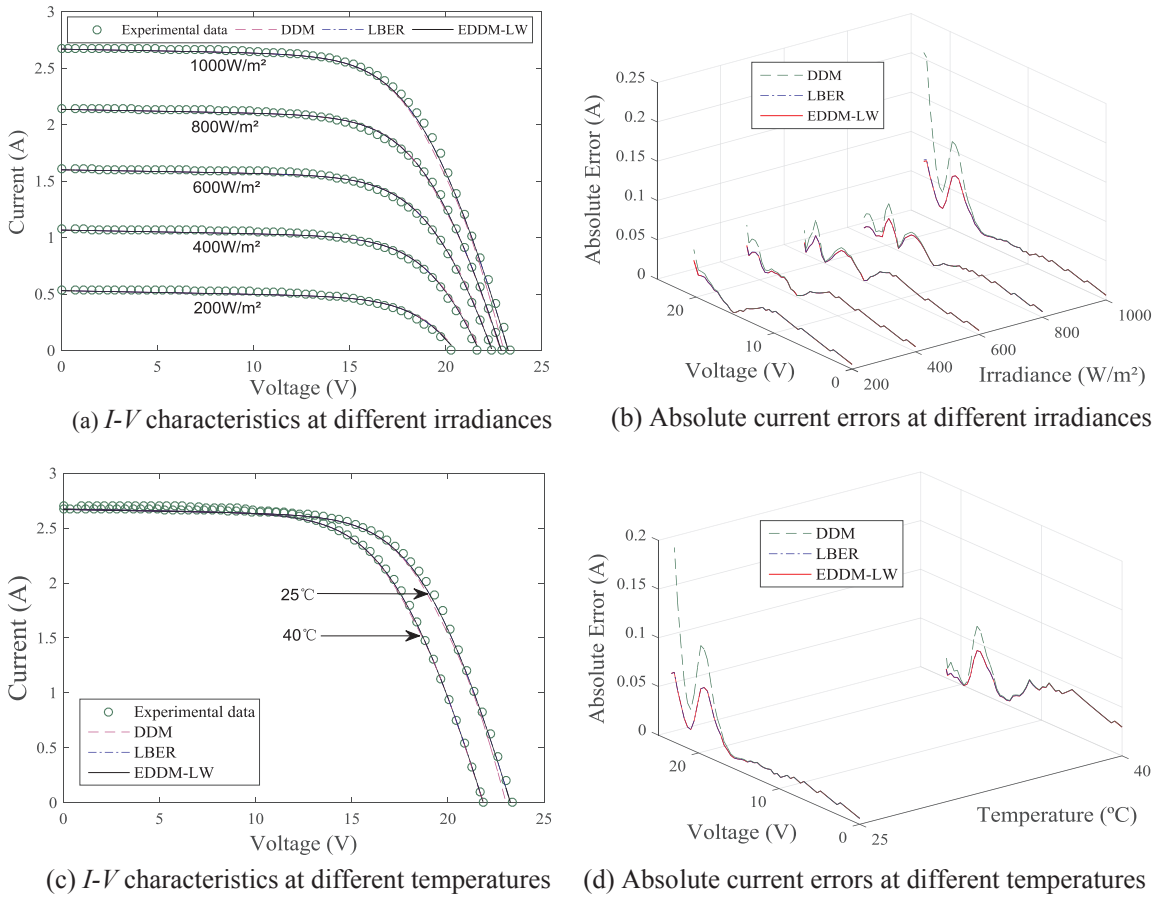

(a) *I-V* characteristics at different irradiances

(b) Absolute current errors at different irradiances

(c) *I-V* characteristics at different temperatures

(d) Absolute current errors at different temperatures

Fig. 8. Calculated curves based on DDM, LBER, and EDDM-LW using the parameter values extracted by FPA for solar module ST40.

$$x_{new1}^{i} = \begin{cases} x_{old}^{i} + rand(0,1) \times (x^{i} - x^{j}), f(x^{i}) < f(x^{j}) \\ x_{old}^{i} - rand(0,1) \times (x^{i} - x^{j}), f(x^{i}) > f(x^{j}) \end{cases} \quad (31)$$

In Eq. (31), each student randomly selects another student to interact with and improve his or her performance using the old individual x_{old}^{i}, thereby resulting in limited learning ability and the convergence rate. Thus, an elite learning strategy [52], as shown in Eq. (32), is introduced to perform local searching. Students improve their performance by the teacher, which is quite close to the global optimum. Therefore, the learning direction can move quickly to the optimal solution.

$$x_{new2}^{i} = x_{teacher} + rand(0,1) \times (x^{i} - x^{r}) \quad (32)$$

Although the elite learning strategy increases the rate of convergence, searching can be easily trapped into the local optimal. In the algorithm, students are expected to rapidly approach the promising region of the search space at the early stage and to improve their local searching ability during the latter optimization process. Therefore, a hybrid learning strategy [53] is introduced, which combines the original learner phase and the elite learning strategy, as implemented in Eq. (33):

$$x_{new3}^{i} = \left(1 - \frac{iter}{iter_{\max}}\right) x_{new1}^{i} + \frac{iter}{iter_{\max}} x_{new2}^{i} \quad (33)$$

In the early stage of the algorithm, *iter* is small, and the original learner phase dominates the optimization process. Random interactive learning among the students ensures population diversity. The coefficient of x_{new1}^{i} increases with the advance of the algorithm. The elite learning strategy then plays a leading role in the optimization process to strengthen the local search ability. The hybrid strategy satisfies the optimal demand of the optimization algorithm at different times and is beneficial for the improvement of the overall performance of the algorithm.

Based on the aforementioned description, the procedure of the ITLBO algorithm is implemented as follows. The flowchart of the ITLBO is presented in Fig. 9.

Step 1: Create *NP* students, and randomly initialize the values of each individual using Eq. (28) from their corresponding search space. Calculate the fitness value RMSE for each individual using the objective function, as presented in Eq. (27).
Step 2: Assign the individual which has the lowest RMSE as the teacher.
Step 3: Teacher phase. Generate a new individual x_{new}^{i} using Eqs. (29) and (30), and calculate the fitness value RMSE. The new individual will replace the old one when it gives a smaller RMSE.
Step 4: Learner phase. Generate two new individuals, specifically x_{new1}^{i} and x_{new2}^{i}, using Eqs. (31) and (32), respectively. The newest self-adapting individual x_{new3}^{i} can then be produced according to Eq. (33). Update the old individual when the RMSE value calculated by x_{new3}^{i} is smaller.
Step 5: Update all the individuals with step 3 and step 4.
Step 6: Stop and output the best solution if the $iter_{max}$ value is reached; otherwise, return to step 2.

5. Parameter extraction for EDDM-LW

This section elaborates the parameter extraction results of EDDM-LW. All the experiments are carried out in MATLAB R2015b.

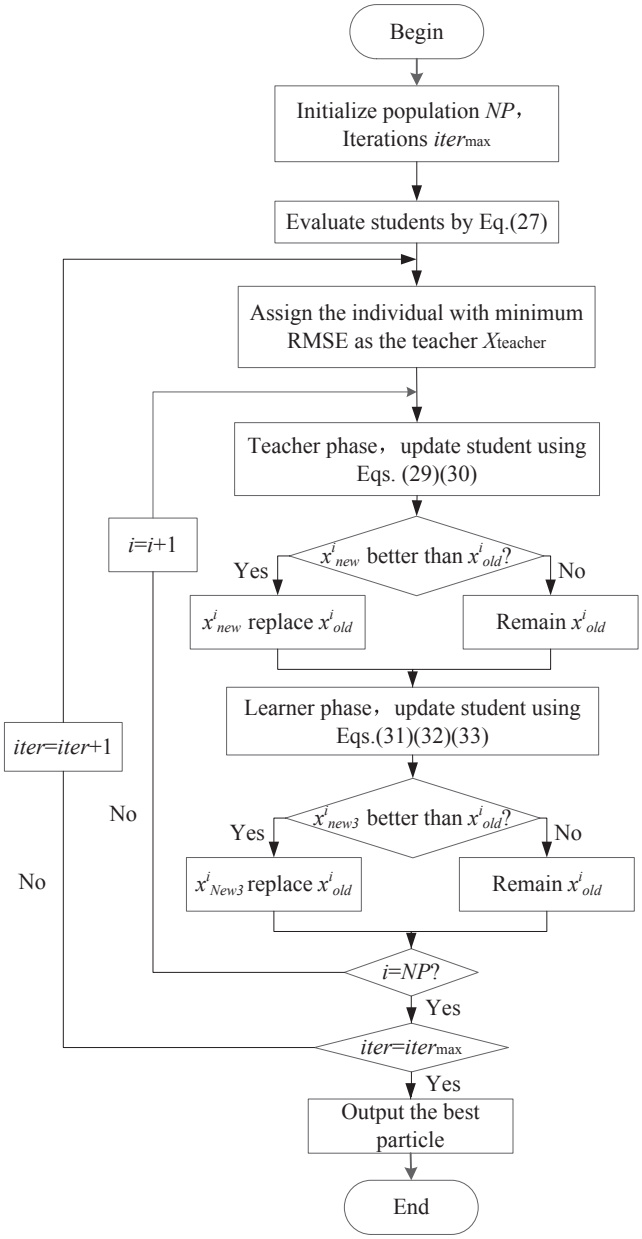

Fig. 9. Flow chart of the improved teaching–learning-based optimization algorithm.

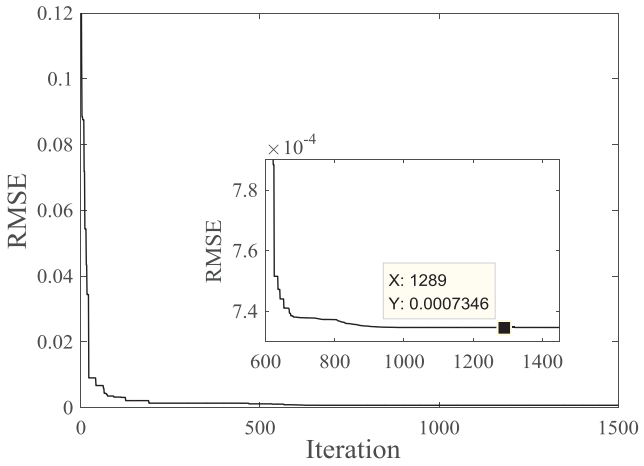

Fig. 10. Convergence curves of the ITLBO.

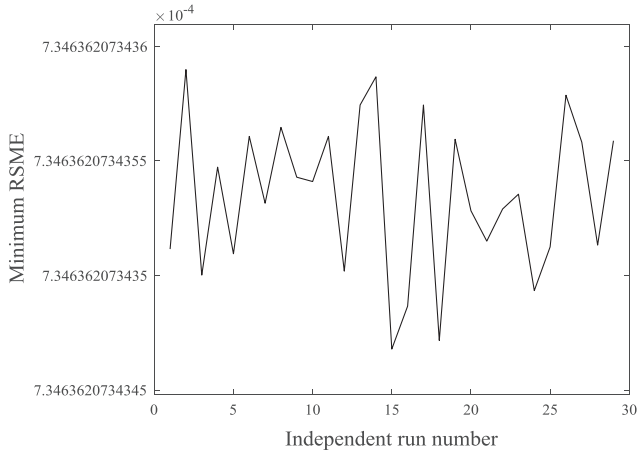

Fig. 11. Distribution of the minimum RMSE value over 30 independent runs.

5.1. Parameter extraction for RTC France solar cell

The parameter search ranges for the RTC France solar cell are set the same as Refs. [40–47]. The number of the population is set to 200, and the maximum iteration of the function evaluations is 2500. The algorithm is tested for 30 independent runs. The best result is listed in Table 6. It is clear that the minimum RMSE value of EDDM-LW (0.000734636) is smaller than that in the literature, as indicated in Table 1. It would be premature to conclude the parameter values extracted from EDDM-LW are more accurate than those from DDM, because there is a remarkable fitness difference between DDM and EDDM-LW.

Fig. 10 presents the best convergence curve of the ITLBO during the parameter extraction of EDDM-LW for the RTC France solar cell. Fig. 11 shows the distribution of the RMSE value over 30 independent runs. The total iteration number is small and the minimum RMSE values of 30 independent runs are stable, thereby indicating that the ITLBO algorithm has good convergence speed and convergence accuracy.

Fig. 12 presents the simulated *I-V* curve and absolute current errors, which are calculated by the parameters extracted from EDDM-LW. The estimated model is quite consistent with the experimental data. All the IAE values are smaller than 1.35E-3, thereby confirming that the optimal parameter values extracted from EDDM-LW are accurate.

5.2. Parameter extraction for solar modules

To examine the samples further, the ITLBO is used to extract the optimal parameters of EDDM-LW for three different types of solar modules (mono-crystalline (SM55) module, multi-crystalline (S75) module, and thin-film (ST40) module). The population is set to 200,

Table 6
Optimal parameter values and RMSE extracted by the ITLBO for the EDDM-LW of the RTC France solar cell.

	I_L(A)	I_{o1}(μA)	I_{o2}(μA)	R_s(Ω)	R_p(Ω)	n_1	n_2	κ	τ	$RMSE_{EDDM-LW}$
Search ranges	[0,1]	[0,1]	[0,1]	[0,0.5]	[0,100]	[1,2]	[1,2]	–	–	–
Parameter values	0.760825	0.085283	0.929486	0.037225	55.972906	1.379941	1.791197	3.4841	−0.0169	7.346362E-04

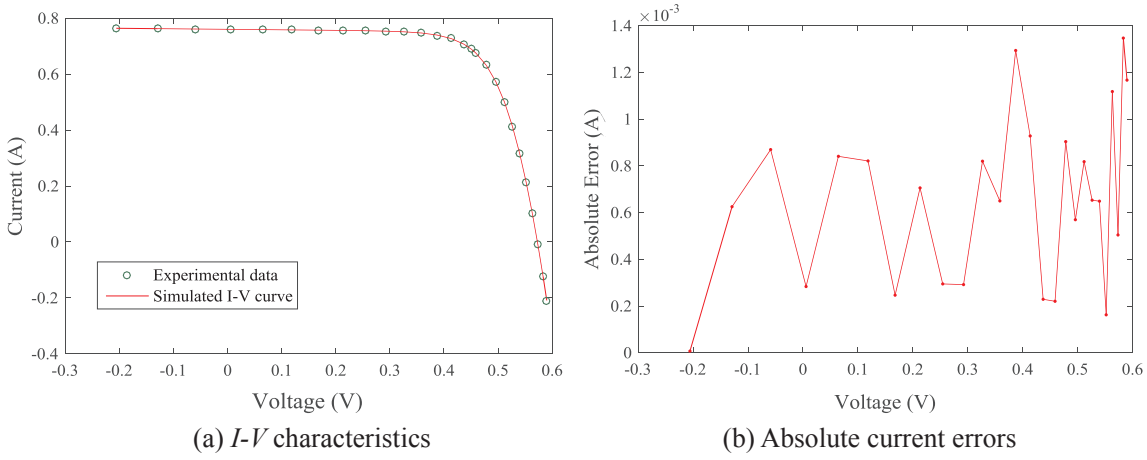

Fig. 12. Simulated curves of EDDM-LW using the optimal parameter values extracted by the ITLBO for the RTC France solar cell.

Table 7
Optimal parameter values and RMSE values extracted by ITLBO for EDDM-LW of solar module SM55 at different irradiance and temperature levels.

Irrad. & Temp.	I_L(A)	I_{o1}(μA)	I_{o2}(μA)	R_s(Ω)	R_p(Ω)	n_1	n_2	κ	τ	$RMSE_{EDDM-LW}$
200 W/m^2,25 °C	0.691945	1.74102E-03	0.017173	0.318865	389.270809	1.165867	1.238130	0.31769	−0.00145	0.0022196
400 W/m^2,25 °C	1.384222	4.53917E-04	0.147030	0.626517	412.017065	1.002218	1.630609	9.03520	−0.02162	0.0046136
600 W/m^2,25 °C	2.076463	2.70551E-04	0.627107	0.616117	402.877301	1.001059	1.984681	45.1810	−0.23154	0.0066669
800 W/m^2,25 °C	2.768692	7.75956E-04	0.066334	0.523096	381.767219	1.050657	1.777790	109.025	−0.19937	0.0084614
1000 W/m^2,25 °C	3.466331	3.08512E-04	0.036952	0.504674	310.926112	1.012780	1.558029	28.7685	−0.16753	0.0117389
1000 W/m^2,20 °C	3.446822	0.99170E-04	0.001085	0.497137	478.271151	1.300247	1.114972	0.00404	0.000201	0.0136719
1000 W/m^2,40 °C	3.473890	8.03896E-03	9.223215	0.496380	385.542814	1.072831	2.129383	16.4092	−0.26284	0.0078372
1000 W/m^2,60 °C	3.485072	5.80462E-02	9.103699	0.485767	399.373313	1.046202	1.654661	4.31709	−0.14881	0.0082001

Table 8
Optimal parameter values and RMSE values extracted by ITLBO for EDDM-LW of solar module S75 at different irradiance and temperature levels.

Irrad. & Temp.	I_L(A)	I_{o1}(μA)	I_{o2}(μA)	R_s(Ω)	R_p(Ω)	n_1	n_2	κ	τ	$RMSE_{EDDM-LW}$
200 W/m^2,25 °C	0.941427	9.70123E-04	0.034875	0.220834	410.63170	1.110208	1.280945	0.35165	−0.00123	0.0025213
400 W/m^2,25 °C	1.879435	6.20065E-03	0.033115	0.245793	400.80640	1.145981	1.438909	9.19531	−0.14596	0.0058345
600 W/m^2,25 °C	2.822312	3.62829E-04	0.364799	0.410620	387.01215	1.002128	2.118397	127.389	−0.07809	0.0124329
800 W/m^2,25 °C	3.755382	3.52459E-04	0.243861	0.394870	386.94160	1.000660	1.994064	117.633	−0.10118	0.0129240
1000 W/m^2,25 °C	4.700360	3.44848E-04	0.705787	0.315935	294.37701	1.005145	1.735098	9.00714	−0.27156	0.0132817
1000 W/m^2,20 °C	4.688601	1.48551E-04	0.060274	0.222684	353.98845	1.173413	1.329352	0.02789	−0.00148	0.0165621
1000 W/m^2,40 °C	4.707125	3.45411E-03	0.539698	0.271541	1498.913	1.307977	1.322699	0.00767	−0.000045	0.0100986
1000 W/m^2,50 °C	4.726315	0.566716	4.375981	0.257702	1615.203	1.274014	1.540567	1.81051	−0.02631	0.0182117
1000 W/m^2,60 °C	4.767251	6.081770	1.365959	0.274062	2332.121	1.368034	1.515242	16.1934	−0.02862	0.0247087

Table 9
Optimal parameter values and RMSE values extracted by ITLBO for EDDM-LW of solar module ST40 at different irradiance and temperature levels.

Irrad.& Temp.	I_L(A)	I_{o1}(μA)	I_{o2}(μA)	R_s(Ω)	R_p(Ω)	n_1	n_2	κ	τ	$RMSE_{EDDM-LW}$
200 W/m^2,25 °C	0.539193	1.044198	77.590828	0.172034	827.72499	1.796106	2.158555	0.07358	−0.00045	0.0026748
400 W/m^2,25 °C	1.077533	0.256772	20.233829	0.758302	527.32175	1.491769	1.882586	0.19391	−0.00238	0.0042348
600 W/m^2,25 °C	1.613991	0.105881	22.653689	1.011427	497.95411	1.338436	1.940630	0.51946	−0.01203	0.0073091
800 W/m^2,25 °C	2.151538	2.298171	17.608908	0.896882	387.96979	1.613539	1.954237	1.22912	−0.01486	0.0085398
1000 W/m^2,25 °C	2.698081	0.018050	2.3397438	1.279482	259.41171	1.165645	1.770226	3.99644	−0.05458	0.0108611
1000 W/m^2,20 °C	2.697476	3.761751	3.1293846	0.878947	285.11734	1.713113	1.789692	2.09273	−0.00563	0.0091730
1000 W/m^2,40 °C	2.722011	3.460855	47.614786	1.092192	296.22374	1.435315	2.188396	6.69389	−0.07755	0.0093618
1000 W/m^2,60 °C	2.743915	14.22604	55.247608	1.105012	376.63581	1.503352	1.579571	0.43261	−0.00366	0.0122128

and the maximum number of function evaluations is set to 3000. 30 independent runs of the ITLBO are executed under the same simulation conditions.

Because the ranges of the parameters influence the accuracy of the results, the search ranges of model parameters are set similarly to those in Refs. [18,31]. The search range of I_L is 0 to double the value of the short-circuit current [0,2ISC] (A). The lower and upper bounds of $I_{o1,2}$ are computed using Eqs. (34) and (35) [54]. The search ranges of the other parameters are set as R_s∈[0, 2] (Ω), R_p∈[0, 5000] (Ω), and $n_{1,2}$∈[1, 4].

$$I_{0\min} = \min\left\{I_{SC}(G,T)\left[\exp\left(\frac{V_{OC}(G,T)}{V_{th}(G,T)}\right)-1\right]^{-1}\right\} \quad (34)$$

$$I_{0\max} = \max\left\{I_{SC}(G,T)\left[\exp\left(\frac{V_{OC}(G,T)}{4V_{th}(G,T)}\right)-1\right]^{-1}\right\} \quad (35)$$

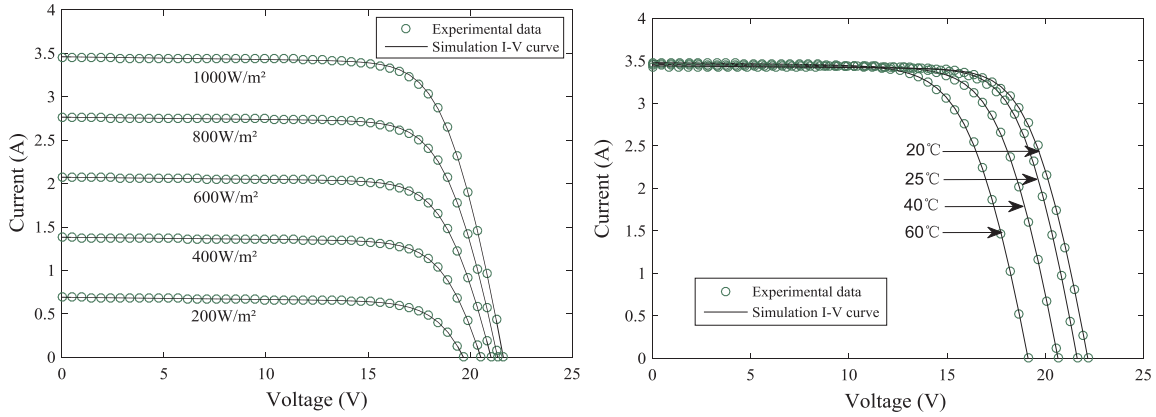

(a) *I-V* characteristics at different irradiances (b) *I-V* characteristics at different temperatures

Fig. 13. Simulated curves of EDDM-LW using the optimal parameter values extracted by ITLBO for solar module SM55.

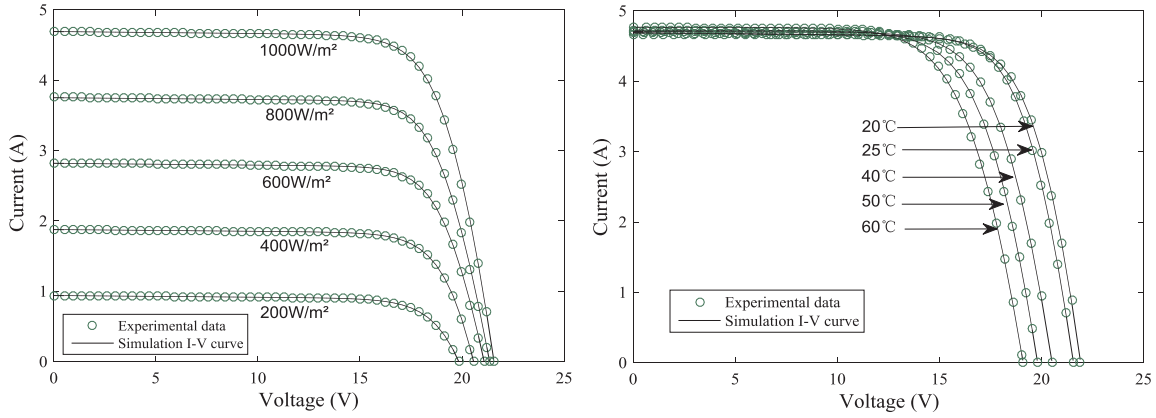

(a) *I-V* characteristics at different irradiances (b) *I-V* characteristics at different temperatures

Fig. 14. Simulated curves of EDDM-LW using the optimal parameter values extracted by ITLBO for solar module S75.

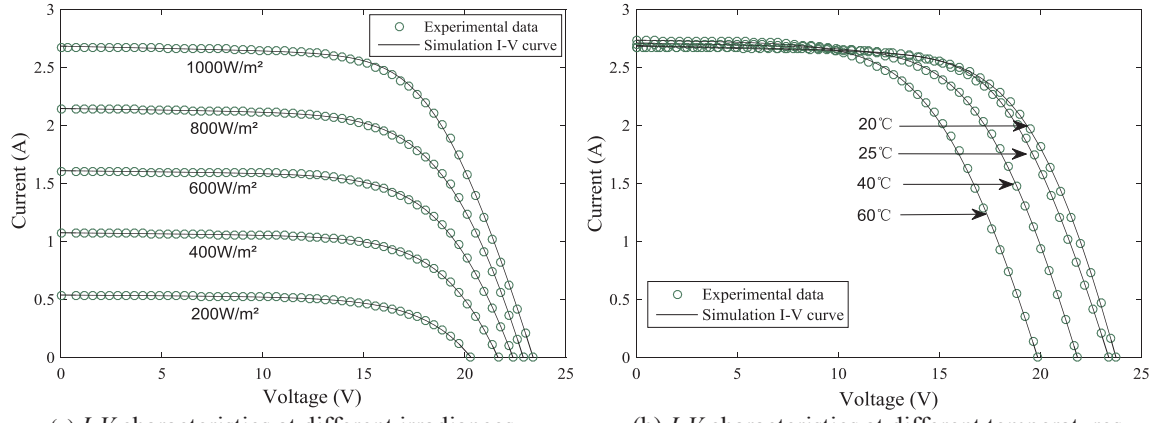

(a) *I-V* characteristics at different irradiances (b) *I-V* characteristics at different temperatures

Fig. 15. Simulated curves of EDDM-LW using the optimal parameter values extracted by ITLBO for solar module ST40.

where I_{SC}, V_{OC} are calculated by Eqs. (10) and (11), respectively.

The optimal parameter values and minimum RMSE values extracted for EDDM-LW of the three solar modules at different irradiances and temperatures are summarized in Tables 7–9. The output currents are calculated by substituting the extracted parameters in EDDM-LW, and the *I-V* characteristics of the three solar modules are plotted at different irradiances and temperatures, as shown in Figs. 13–15.

It is clear that the calculated *I-V* curves of the parameters extracted from EDDM-LW strongly agree with the experimental data at all irradiance and temperature levels. In particular, the accuracies at low irradiances match almost perfectly. Furthermore, the RMSE values calculated with the extracted parameters of EDDM-LW are compared with those in Tables 3–5. The RMSE values exhibit reductions of more than 10%, thereby confirming that the optimal parameter values extracted from EDDM-LW are more accurate than those extracted from DDM. Similar to Refs. [18,31,40], the RMSE values tend to decrease following the decrease in irradiance. It is shown that the parameters extract under low irradiation are more accurate. Accurate parameter

values at low irradiance are crucial when the module is subjected to certain mismatch conditions, such as partial shading [16].

6. Conclusion

This paper presents an improved explicit double-diode model for solar cells. Two new parameters (κ and τ) are defined to separate the two exponential functions in DDM. With the help of the Lambert W function, then an exact explicit *I-V* expression for double-diode model is proposed. To verify the accuracy, the fitness in relation to the experiment *I-V* data and parameter extraction performance are investigated, respectively. The results of the comparisons demonstrate that the proposed model EDDM-LW achieves better fitness in representing the *I-V* characteristics, and the optimal parameters can be extracted accurately from EDDM-LW. With EDDM-LW, for any value of voltage *V* the corresponding exact value of current *I* can be calculated straightforwardly. This calculation generates a higher numeric computational efficiency in the simulation application. Furthermore, the explicit model allows for the straightforward calculation of the maximum power point, which can be used for MPPT algorithms verification. Thus, the proposed model is a useful and practical model for the simulation, evaluation, and optimization of the PV system.

Acknowledgment

The authors would like to thank the anonymous reviewers for their constructive comments, which improved the quality of this paper. This work was supported by the National Natural Science Foundation of China (Grant No. 51478258, 51405287), Shanghai Committee of Science and Technology (Grant No. 18030501300).

References

[1] Ram J Prasanth, Babu T Sudhakar, Dragicevic Tomislav, Rajasekar N. A new hybrid bee pollinator flower pollination algorithm for solar PV parameter estimation. Energy Convers Manage 2017;135:463–76.
[2] Peng Lele, Sun Yize, Meng Zhuo, Wang Yuling, Xu Yang. A new method for determining the characteristics of solar cells. J Power Sources 2013;227:131–6.
[3] Ayop Razman, Tan Chee Wei. A comprehensive review on photovoltaic emulator. Renew Sustain Energy Rev 2017;80:430–52.
[4] Tang Shiqing, Sun Yize, Chen Yujie, Zhao Yiman, Yang Yunhu, Szeto Warren. An enhanced MPPT method combining fractional-order and fuzzy logic control. IEEE J Photovoltaics 2017;7:640–50.
[5] Nassar-eddine I, Obbadi A, Errami Y, El fajri A, Agunaou M. Parameter estimation of photovoltaic modules using iterative method and the Lambert W function: a comparative study. Energy Convers Manage 2016;119:37–48.
[6] Humada Ali M, Hojabri Mojgan, Mekhilef Saad, Hamada Hussein M. Solar cell parameters extraction based on single and double-diode models: a review. Renew Sustain Energy Rev 2016;56:494–509.
[7] Chin Vun Jack, Salam Zainal, Ishaque Kashif. An accurate modelling of the two-diode model of PV module using a hybrid solution based on differential evolution. Energy Convers Manage 2016;124:42–50.
[8] Gao Xiankun, Cui Yan, Hu Jianjun, Xu Guangyin, Wang Zhenfeng, Qu Jianhua, et al. Parameter extraction of solar cell models using improved shuffled complex evolution algorithm. Energy Convers Manage 2018;157:460–79.
[9] Chin Vun Jack, Salam Zainal, Ishaque Kashif. Cell modelling and model parameters estimation techniques for photovoltaic simulator application: a review. Appl Energy 2015;154:500–19.
[10] Pillai Dhanup S, Rajasekar N. Metaheuristic algorithms for PV parameter identification: a comprehensive review with an application to threshold setting for fault detection in PV systems. Renew Sustain Energy Rev 2017;82:3503–25.
[11] Ishaque Kashif, Salam Zainal, Taheri Hamed. Simple, fast and accurate two-diode model for photovoltaic modules. Sol Energy Mater Sol Cells 2011;95:586–94.
[12] Babu B Chitti, Gurjar Suresh. A novel simplified two-diode model of photovoltaic (PV) module. IEEE J Photovoltaics 2014;4:1156–61.
[13] Hejri Mohammad, Mokhtari Hossein, Azizian Mohammad Reza, Ghandhari Mehrdad, Soder Lennart. On the parameter extraction of a five-parameter double-diode model of photovoltaic cells and modules. IEEE J Photovoltaics 2014;4:915–23.
[14] El-Naggar KM, AlRashidi MR, AlHajri MF, Al-Othman AK. Simulated annealing algorithm for photovoltaic parameters identification. Sol Energy 2012;86:266–74.
[15] Ishaque Kashif, Salam Zainal. An improved modeling method to determine the model parameters of photovoltaic (PV) modules using differential evolution (DE). Sol Energy 2011;85:2349–59.
[16] Ishaque Kashif, Salam Zainal, Mekhilef Saad, Shamsudin Amir. Parameter extraction of solar photovoltaic modules using penalty-based differential evolution. Appl Energy 2012;99:297–308.
[17] Askarzadeh Alireza, Rezazadeh Alireza. Artificial bee swarm optimization algorithm for parameters identification of solar cell models. Appl Energy 2013;102:943–9.
[18] Alam DF, Yousri DA, Eteiba MB. Flower pollination algorithm based solar PV parameter estimation. Energy Convers Manage 2015;101:410–22.
[19] Askarzadeh Alireza, Coelho Leandro Dos Santos. Determination of photovoltaic modules parameters at different operating conditions using a novel bird mating optimizer approach. Energy Convers Manage 2015;89:608–14.
[20] Khanna Vandana, Das BK, Bisht Dinesh, Vandana Singh PK. A three diode model for industrial solar cells and estimation of solar cell parameters using PSO algorithm. Renewable Energy 2015;78:105–13.
[21] Oliva Diego, Cuevas Erik, Pajares Gonzalo. Parameter identification of solar cells using artificial bee colony optimization. Energy 2014;72:93–102.
[22] Yuan Xiaofang, He Yuqing, Liu Liangjiang. Parameter extraction of solar cell models using chaotic asexual reproduction optimization. Neural Comput Appl 2015;26:1227–39.
[23] Lin Peijie, Cheng Shuying, Yeh Weichang, Chen Zhicong, Wu Lijun. Parameters extraction of solar cell models using a modified simplified swarm optimization algorithm. Sol Energy 2017;144:594–603.
[24] Xu Yonghai, Kong Xiangyu, Zeng Yawen, Tao Shun, Xiao Xiangning. A modeling method for photovoltaic cells using explicit equations and optimization algorithm. Int J Electr Power Energy Syst 2014;59:23–8.
[25] Fathabadi Hassan. Lambert W function-based technique for tracking the maximum power point of PV modules connected in various configurations. Renewable Energy 2015;74:214–26.
[26] Pindado Santiago, Cubas Javier, Manuel Carlos De. Explicit expressions for solar panel equivalent circuit parameters based on analytical formulation and the Lambert W-Function. Energies 2014;7:4098–115.
[27] Lu-Munoz Denise, Muci Juan, Ort-Conde Adelmo, Garcia-Sanchez Francisco J, de Souza Michelly, Pavanello Marcelo A. An explicit multi-exponential model for semiconductor junctions with series and shunt resistances. Microelectron Reliab 2011;51:2044–8.
[28] Ortiz-Conde Adelmo, Lugo-Muñoz Denise, García-Sánchez Francisco J. An explicit multiexponential model as an alternative to traditional solar cell models with series and shunt resistances. IEEE J Photovoltaics 2012;2:261–8.
[29] Lun Shu-xian, Wang Shuo, Yang Gui-hong, Guo Ting-ting. A new explicit double-diode modeling method based on Lambert W-function for photovoltaic arrays. Sol Energy 2015;116:69–82.
[30] Dehghanzadeh Ahmad, Farahani Gholamreza, Maboodi Mohsen. A novel approximate explicit double-diode model of solar cells for use in simulation studies. Renewable Energy 2017;103:468–77.
[31] Gao Xiankun, Cui Yan, Hu Jianjun, Xu Guangyin, Yu Yongchang. Lambert W-function based exact representation for double diode model of solar cells: comparison on fitness and parameter extraction. Energy Convers Manage 2016;127:443–60.
[32] Easwarakhanthan T, Bottin J, Bouhouch I, Boutrit C. Nonlinear minimization algorithm for determining the solar cell parameters with microcomputers. Int J Solar Energy 1986;4:1–12.
[33] SM55 module. < http://www.solar-bazaar.com/productis/Shell-SM55-Photovoltaic-Solar-Module.pdf > .
[34] S75 module. http://www.aeet-service.com/pdf/shell/Shell-Solar_S75.pdf.
[35] ST40 module. http://www.aeet-service.com/pdf/shell/Shell-Solar_ST40.pdf.
[36] Wolf M, Noel GT, Stirn Richard J. Investigation of the double exponential in the current-voltage characteristics of silicon solar cells. IEEE Trans Electron Devices 1976;24:419–28.
[37] Pavan AM, Vergura S, Mellit A, Lughi V. Explicit empirical model for photovoltaic devices. Exp Validation Sol Energy 2017;155:647–53.
[38] Alqahtani Ayedh H. A simplified and accurate photovoltaic module parameters extraction approach using matlab. In: IEEE International symposium on industrial electronics, 2012, p. 1748–53.
[39] Jain Amit, Kapoor Avinashi. Exact analytical solutions of the parameters of real solar cells using Lambert W -function. Sol Energy Mater Sol Cells 2004;81:269–77.
[40] Xu Shuhui, Wang Yong. Parameter estimation of photovoltaic modules using a hybrid flower pollination algorithm. Energy Convers Manage 2017;144:53–68.
[41] Gong Wenyin, Cai Zhihua. Parameter extraction of solar cell models using repaired adaptive differential evolution. Sol Energy 2013;94:209–20.
[42] Guo Lei, Meng Zhuo, Sun Yize, Wang Libiao. Parameter identification and sensitivity analysis of solar cell models with cat swarm optimization algorithm. Energy Convers Manage 2016;108:520–8.
[43] Askarzadeh Alireza, Rezazadeh Alireza. Extraction of maximum power point in solar cells using bird mating optimizer-based parameters identification approach. Sol Energy 2013;90:123–33.
[44] Yu Kunjie, Chen Xu, Wang Xin, Wang Zhenlei. Parameters identification of photovoltaic models using self-adaptive teaching-learning-based optimization. Energy Convers Manage 2017;145:233–46.
[45] Chen Xu, Yu Kunjie, Du Wenli, Zhao Wenxiang, Liu Guohai. Parameters identification of solar cell models using generalized oppositional teaching learning based optimization. Energy 2016;99:170–80.
[46] Askarzadeh Alireza, Rezazadeh Alireza. Parameter identification for solar cell models using harmony search-based algorithms. Sol Energy 2012;86:3241–9.
[47] Derick M, Rani C, Rajesh M, Farrag ME, Wang Y, Busawon K. An improved optimization technique for estimation of solar photovoltaic parameters. Sol Energy 2017;157:116–24.
[48] Rao RV, Savsani VJ, Vakharia DP. Teaching-learning-based optimization: a novel

method for constrained mechanical design optimization problems. Comput Aided Des 2011;43:303–15.
[49] Chen Debao, Zou Feng, Wang Jiangtao, Yuan Wujie. A teaching-–learning-based optimization algorithm with producer-–scrounger model for global optimization. Soft Comput 2015;19:745–62.
[50] Lotfipour Arash, Afrakhte Hossein. A discrete teaching–learning-based optimization algorithm to solve distribution system reconfiguration in presence of distributed generation. Int J Electr Power Energy Syst 2016;82:264–73.
[51] Rao R Venkata, Patel Vivek. Multi-objective optimization of heat exchangers using a modified teaching-learning-based optimization algorithm. Appl Math Model 2013;37:1147–62.
[52] Niu Qun, Zhang Hongyun, Li Kang. An improved TLBO with elite strategy for parameters identification of PEM fuel cell and solar cell models. Int J Hydrogen Energy 2014;39:3837–54.
[53] Bi Xiaojun, Wang Jiahui. Teaching-learning-based optimization algorithm with hybrid learning strategy. J Zhejiang Univ(Eng Sci) 2017;51:1024–31.
[54] Villalva Marcelo Gradella, Gazoli Jonas Rafael, Ruppert Filho Ernesto. Comprehensive approach to modeling and simulation of photovoltaic arrays. IEEE Trans Power Electron 2009;24:1198–208.